An Analysis of Long Baseline Radio Interferometry, Part III

J. B. Thomas
Tracking and Orbit Determination Section

This article is the third installment in a series of articles presenting an analysis of long baseline radio interferometry. The practical data reduction steps that are required to extract fringe amplitude, fringe phase, and delay are described. These data reduction steps include bit stream manipulations, fringe stopping, Fourier analysis, and phase tracking. In addition, a detailed analysis is presented for the two-channel approach to bandwidth synthesis, a technique used for making accurate delay measurements.

I. Introduction

Two previous articles (Refs. 1, 2) were the first of a series of technical reports presenting an analysis of long baseline radio interferometry. In those reports, the cross-correlation function for a natural radio source was expressed in terms of fringe visibility, system temperatures, fringe phase and delay. In addition, an approximate mathematical model for the geometric delay (Ref. 1) was outlined. This report describes the practical steps in data reduction that are required to extract fringe amplitude, fringe phase, and delay. Fringe amplitude measurements can yield valuable information concerning source structure (Ref. 1). Delay and fringe phase measurements can lead to precise determination of geophysical parameters (polar motion, UT1, baseline vectors) and radio source locations. The data reduction steps described in this report include bit stream manipulations, fringe stopping, Fourier analysis, and phase tracking. In addition, the last section outlines two-channel bandwidth synthesis, a technique used for making accurate delay measurements.

II. Cross-Correlated Function

In long baseline interferometry measurements, the radio signal produced by a distant source is recorded simultaneously at two widely spaced antennas. These recorded signals are then cross-correlated to determine correlated amplitude as well as delay and fringe phase. In the present radio interferometry data reduction system, the first step in cross-correlation involves the multiplication of the voltage signals observed at the two antennas. One signal is offset in time to compensate for the difference in wave front arrival times.

Previous reports (Refs. 1, 2) derive the ensemble average of the voltage product for a natural source. This average voltage product, called the cross-correlation function (CCF), is given for analog signals by the expression (Ref. 2):

$$r_a(t, \tau_m) \equiv \frac{\langle V_1(t)\, V_2(t+\tau_m)\rangle}{\sqrt{\langle V_1^2\rangle \langle V_2^2\rangle}} = \gamma_v \sqrt{\frac{T_{R_1} T_{R_2}}{T_{S_1} T_{S_2}}} \frac{W_D}{W_B} \frac{\sin \pi W_D \Delta\tau_r}{W_D \Delta\tau_r} \cos\phi_f \tag{1}$$

where fringe phase is given by

$$\phi_f = (\omega_2 - \omega_1)\, t + \omega_2 \tau_m + \omega_a (\tau_g + \tau_I + \tau_c + \tau_t - \tau_m) + I_a + R_a + C_a$$

and where the "time delay error" is given by

$$\Delta\tau_r = \tau_g + \tau_I + \tau_c + \tau_t - \tau_m$$

In this expression,

$V_j(t)$ = voltage recorded at time t at station $j, j = 1, 2$

γ_v = fringe visibility

T_{R_j} = radio source temperature at station j

T_{S_j} = system noise temperature at station j

W_B = instantaneous recorded bandwidth

W_D = bandpass overlap after doppler shifting

ω_j = total effective mixing frequency at station $j, j = 1, 2$

ω_a = effective interferometer bandpass center after doppler shifting

I_a = total instrumental phase shift including mixing signal drifts

R_a = brightness transform phase shift

τ_m = model time delay, computed

τ_g = geometric time delay, actual

τ_I = total instrumental delay including clock synchronization error

τ_t = differential troposphere time delay

τ_c = differential charged-particle time delay at frequency ω_a

C_a = differential charged-particle phase shift at frequency ω_a

Note that transmission media effects have been included in the total delay and phase for completeness. This expression assumes a rectangular system bandpass with a linear phase-frequency response at each station. The model delay τ_m contains best estimates for the geometric and instrumental delays. In some cases, a troposphere model might be included in τ_m. In addition to these terms, the model delay always contains a time-independent offset τ_V which can be adjusted to "fine-tune" the alignment of the two bit streams.

The present JPL interferometry system is not analog but digital and records only the sign of the voltage signals. For such infinitely clipped signals, the cross-correlation function becomes (Refs. 2, 3):

$$r_a(t, \tau_m) \equiv \langle \tilde{V}_1(t)\, \tilde{V}_2(t+\tau_m)\rangle = \frac{2}{\pi} \sin^{-1} r_a(t, \tau_m) \tag{2}$$

where

$$\tilde{V}_j(t) = +1 \text{ if } V_j(t) > 0$$

$$\tilde{V}_j(t) = -1 \text{ if } V_j(t) < 0$$

In this report, we will consider only the weak source case ($r_a << 1$) for which

$$r_a(t, \tau_m) = \frac{2}{\pi} r_a(t, \tau_m) = A_f \cos\phi_f \tag{3}$$

where

$$A_f = \frac{2}{\pi} \gamma_v \sqrt{\frac{T_{R_1} T_{R_2}}{T_{S_1} T_{S_2}}} \frac{W_D}{W_B} \frac{\sin \pi W_D \Delta\tau_r}{\pi W_D \Delta\tau_r}$$

The cross-correlation function describes the average behavior of the voltage product. As indicated by Eq. (3), the cross-correlation function is a product of a sinusoidal factor $\cos\phi_f$ and an amplitude factor A_f. The phase of the sinusoidal factor describes the average phase behavior of the total system. The amplitude factor is a measure of the accuracy of time domain alignment and peaks if the model delay τ_m is sufficiently close to the actual total group delay ($W_D \Delta\tau_r << 1$). In addition, the amplitude depends on the source's correlated flux and system noise.

The next section will describe how, on the basis of this expected average behavior, the actual voltage products

are formed and manipulated so that amplitude, phase, and delay can eventually be extracted. Fringe amplitude measurements can yield valuable information concerning source structure (Ref. 1). Delay and fringe phase measurements can lead to precise determination of Earth orientation parameters, baseline vectors, and radio source locations.

III. Bit Stream Manipulations

The voltage signals at each antenna are sampled in time at the Nyquist rate $2W_B$, where W_B is the instantaneous recorded bandwidth. The volume of data generated by typical sampling rates (10^4–10^6 bits/sec) is too large to be manageable without compression. In addition, the noise on a single sample point on the cross-correlation function is generally too large for a single point to be informative when taken alone. Consequently, data compression techniques are employed in order to both reduce the volume of data and to collect statistics. The compressed data reveal the underlying characteristics of the cross-correlation function that are totally masked by noise over a few sample points. Typically, one data point in the compressed data (stopped fringes) contains 10^4–10^6 original sample points. Two stages are involved in the data compression procedure: presums and fringe stopping. The basic features of the initial steps in data reduction (signal multiplication and presums) will now be outlined. Fringe stopping is discussed in Section IV.

In a digital recording system, a positive voltage obtained at a given sample point is represented on tape by a bit with value 1 while a negative voltage is a 0 bit. Examples of two such bit streams, one for each antenna, are shown in Fig. 1. As indicated earlier, the time spacing between adjacent bits is $1/(2W_B)$ where W_B is the instantaneous bandwidth. After being read into a computer, bit stream 2 is offset relative to bit stream 1 by a model delay τ_m which partially compensates for the time delay of signal 2. The model delay is typically a sum of a time-varying geometric delay, a constant instrumental delay and an adjustable offset (τ_v). Because the time scale is quantized in bits, the total time offset τ_m can at best be rounded to the nearest bit. For typical experiments the quantized time offset ($\bar{\tau}_m$) is constant over many bits in time before the model delay τ_m changes by one bit ($\dot{\tau}_m \lesssim 2\mu$bits/bit). Consequently, many bits require the same quantized time offset and may be aligned simultaneously by one shift operation. The bit streams are then multiplied together by means of an EXCLUSIVE OR, a digital logic operation that can operate simultaneously on all bits in a word of data (32 bits in an IBM 360). The fact that many bits may be shifted and multiplied simultaneously greatly reduces computation time. In the EXCLUSIVE OR operation the following rules are satisfied:

$$1*0=0 \qquad 1*1=1$$

$$0*1=0 \qquad 0*0=1$$

One can readily show that these relations produce a product with the proper sign when decoded under the bit conventions defined above. An example of bit multiplication for 8 bits is shown in Fig. 1 along with the corresponding sign interpretation for the process.

Since the time offset must be quantized and rounded to the nearest bit, the two bit streams can not be perfectly aligned for all bits. This roundoff misalignment in digital systems smears the "analog" delay curve. The resultant loss in peak amplitude is easily calculated by averaging the expected delay curve over ± 0.5 bits about the principal maximum. In this manner, one can readily show that a loss of peak amplitude of 3.4% results for an "ideal" $\sin(x)/x$ curve. In subsequent work, this slight roundoff smearing effect will be neglected.

After multiplication of the two bit streams, one has obtained over a limited time range a function that on the average is given by the cross-correlation function in Eq. (3). If the frequency $\dot{\phi}_f$ is small enough ($\approx 2 - 100$ Hz) and the recording rate is large ($\approx 10^4$ to 10^6 bits/sec) the CCF will be sampled many times (10^2 to 10^5) during one cycle of fringe phase as schematically indicated in Fig. 2. (The magnitude of the fringe frequency $\dot{\phi}_f$ may be greatly reduced by proper selection of mixing frequencies, ω_1 and ω_2, during the measurement.) Without loss of information concerning the CCF, one can sum adjacent sample points as long as the sum time interval is small (~ 0.1 cycle) compared to one cycle of fringe phase. These local sums are called presums. A simple example is given for 8 bits in Fig. 1. As indicated by the ostensibly random bits in this example, the systematic trends of the CCF are usually not evident over only a few bits due to poor SNR.

Because of the 0.1 cycle constraint, the presums for the present 48 kbits/s system cover time intervals ranging from one word (32 bits) to 50 words. Since the presums are carried over only a fraction of a cycle, each presum can be regarded as the value of the CCF at the middle of the presum interval multiplied by the number of bits in the presum. Thus, after signal multiplication and presum, the resulting CCF is identical to the original CCF (Eq. 3),

except for an amplitude increase, and is sampled less frequently. The presums $U_p(t, \tau_m)$ can formally be represented as

$$U_p(t, \tau_m) = \sum_{t' = t - \Delta t_p/2}^{t' = t + \Delta t_p/2} \tilde{V}_1(t') \tilde{V}_2(t' + \tilde{\tau}_m) \qquad (4)$$

where $\tilde{V}_j$ denotes infinitely clipped voltage and Δt_p is the presum time interval. All bit products within this time interval are included in the sum. The expected behavior of the presums is given by the expression

$$U_p(t, \tau_m) = N_t A_f \cos \phi_f + \text{noise} \qquad (5)$$

where N_t is the number of bits in the presum given by

$$N_t = 2W_B \Delta t_p$$

Generally, the noise on the presums is too large for an individual presum to be useful. Therefore, the data must be compressed even more to reveal the cross-correlation function as indicated in the next section.

IV. Fringe Stopping

After obtaining the presums, the data can be compressed more by a process known as fringe stopping or phase counter-rotation. The first step in this process multiplies the presums by the cosine (or sine) of a model phase. (In the present system, the fringes are stopped with both the sine and cosine functions so that two statistically independent fringe compressions are obtained.) The model phase is computed from the expression

$$\phi_m(t) = -\varepsilon t + (\omega_2' - \omega_1') t + \omega_2' \tau_m \qquad (6)$$

where ω_1' and ω_2' are best estimates for the mixing frequencies ω_1, and ω_2 and τ_m is the model delay discussed in Section II. The frequency ε is a small analytical offset ($\approx 0.1 - 0.2$ Hz) of known sign and magnitude that will be discussed below. When the presums are multiplied by the cosine of the model phase, one obtains two terms

$$\begin{aligned} U_p(t, \tau_m) \cos \phi_m &= N_t A_f \cos \phi_f \cos \phi_m + \text{noise} \\ &= \frac{1}{2} N_t A_f [\cos(\phi_f - \phi_m) + \cos(\phi_f + \phi_m)] \\ &\quad + \text{noise} \end{aligned} \qquad (7)$$

The first term is of low frequency if the model phase closely approximates the actual phase ϕ_f. As indicated by Eqs. (1) and (6), this phase difference (stopped phase) is given by

$$\phi_f - \phi_m = \varepsilon t + \Delta\omega_a t + \omega_a \Delta\tau_r' + I_a + R_a + C_a \qquad (8)$$

where

$$\Delta\omega_a \equiv \omega_2 - \omega_1 - \omega_2' + \omega_1'$$

$$\Delta\tau_r' \equiv \tau_g + \tau_I + \tau_t - \tau_m$$

We have assumed the $(\omega_2 - \omega_2')\tau_m$ term is negligibly small, which is usually the case for typical frequency calibration accuracies ($\Delta f/f \approx 10^{-12}$).

Typically, residual frequencies in $\dot{\phi}_f - \dot{\phi}_m$ due to model errors in τ_m, ω_1' and ω_2' are less than 0.2 Hz at S-band. The second term in Eq. (7) has a frequency roughly equal to $2\dot{\phi}_f$ which typically falls in the range 5 to 200 Hz. Thus, a sum over time intervals that are small (~ 0.1 cycle) compared to the cycle time of $\phi_f - \phi_m$ will increase the amplitude of the first term but will leave it unmodified otherwise. However, such a sum will generally average the second term over enough cycles (~ 5) to make it negligibly small. These sum intervals are typically 0.1 to 1.0 seconds long. Fringe stopping can be formally represented as the sum

$$U_S(t, \tau_m) \equiv \sum_{t' = t - \Delta t_s/2}^{t' = t + \Delta t_s/2} U_p(t', \tau_m) \cos \phi_m(t') \qquad (9)$$

where Δt_s is the sum interval length. All presums within this interval are included in the sum. The expected form for these "stopped fringes" is given by the expression

$$U_S(t, \tau_m) = \frac{1}{2} N_S A_f \cos(\phi_f - \phi_m) + \text{noise} \qquad (10)$$

where $N_S = 2W_B \Delta t_s$ is the number of bits in the interval Δt_s.

In the present system, the stopped fringes are divided by the "known" factor

$$K_N = \frac{1}{\pi} \frac{W_D}{W_B} N_s \qquad (11)$$

so that the maximum fringe amplitude depends only on correlated flux and noise temperatures. The normalized stopped fringes are computed by the expression

$$U_N(t, \tau_m) = U_s(t, \tau_m)/K_N \qquad (12)$$

The expected behavior of the normalized fringes is given by the expression

$$U_N(t, \tau_m) = A_N \cos(\phi_f - \phi_m) + \text{noise} \qquad (13)$$

where

$$A_N = \gamma_v \sqrt{\frac{T_{R_1} T_{R_2}}{T_{S_1} T_{S_2}}} \frac{\sin \pi W_D \Delta\tau_r}{\pi W_D \Delta\tau_r}$$

With this normalization, the maximum fringe amplitude is theoretically given by

$$A_N|_{\max} = \gamma_v \sqrt{\frac{T_{R_1} T_{R_2}}{T_{S_1} T_{S_2}}} \qquad (14)$$

and therefore depends only on the magnitude of the "correlated flux temperatures" relative to the system noise temperatures. Thus, the stopped fringes are sampled every Δt_s seconds (0.1 to 1 sec) and possess the "stopped" fringe frequency $\dot{\phi}_f - \dot{\phi}_m$ ($\lesssim$ 0.2 Hz at S-band).

The stopped fringe frequency (See Eq. 8) is a sum of two components—the analytical offset ε and the residual fringe frequency $\Delta\nu_a$

$$\dot{\phi}_f - \dot{\phi}_m = \varepsilon + \Delta\nu_a \qquad (15)$$

where

$$\Delta\nu_a \equiv \Delta\omega_a + \omega_a \Delta\dot{\tau}'_r + \dot{I}_a + \dot{R}_a + \dot{C}_a$$

The residual fringe frequency $\Delta\nu_a$ is the unknown frequency due to all physical effects that remain after the model $\omega_a \dot{\tau}_m$ (contained in $\omega_a \Delta\dot{\tau}'_r$) has been subtracted. The known offset ε is a computational artifact designed to resolve the frequency sign ambiguity. The sign ambiguity is a consequence of the fact that only the magnitude of frequency can be extracted from a sinusoid. The magnitude of ε is chosen so that it is larger than the maximum expected magnitude of the residual fringe frequency $\Delta\nu_a$ including all physical effects. If ε is this large, then the sign of $\Delta\nu_a$ can be determined by noting the sense of the total output frequency $|\dot{\phi}_f - \dot{\phi}_m|$ relative to $|\varepsilon|$. For example, assume that $\varepsilon = +0.2$ Hz. If $\Delta\nu_a$ is negative in Eq. (15), then it is subtracted from ε and $|\dot{\phi}_f - \dot{\phi}_m|$ is less than ε. If $\Delta\nu_a$ is positive, then $|\dot{\phi}_f - \dot{\phi}_m|$ is larger than ε. Therefore, if $|\dot{\phi}_f - \dot{\phi}_m| = 0.25$ Hz, then $\Delta\nu_a = 0.05$ Hz. If $|\dot{\phi}_f - \dot{\phi}_m| = 0.15$ Hz, then $\Delta\nu_a = -0.05$ Hz.

The various contributions to the residual frequency $\Delta\nu_a$ may be bounded as follows. As indicated earlier, the mixing frequencies are usually known to within 20 mHz at S-band. The residual frequency due to parameter errors in the model geometric delay can be bounded by means of the maximum values (Ref. 4) of the sensitivity partials[1] which for S-band observations over intercontinental baselines ($\approx$ 10,000 km) are given by

$$\frac{\partial\nu_g}{\partial x} \sim 0.5 \text{ mHz/m} \qquad \frac{\partial\nu_g}{\partial\theta} \sim 20 \text{ mHz/arc sec} \qquad (16)$$

where x and θ symbolize length and angle parameters, respectively. For example, if source location errors are less than 5 arc sec, the residual frequency due to this error source is less than 100 mHz. The single-raypath troposphere frequency effect ($\omega_a \dot{\tau}_t$) at S-band is less than 30 mHz for elevation angles greater than 10 deg. This transmission media effect can be largely eliminated (90%) by including existing troposphere models in τ_m. Ionosphere frequency effects at S-band are generally below 5 mHz.

An example of stopped fringes obtained over a Goldstone baseline with a 48 kbits/sec recording system[2] is shown in Fig. 3 for nine delay offsets. For the narrowband recording system in this example, the *a priori* delay was accurate enough to align the two bit streams within a fraction of a bit. Variations about the *a priori* delay were produced by assigning the adjustable offset τ_V the indicated values. Note that the amplitude variation of the fringes as a function of *time offset* fairly closely approximates the sin $(x)/x$ width ($\approx$ 40 μs) predicted by Eq. (13). As explained in Section VI, this amplitude variation versus model delay can be used to extract the single-channel delay observable. The frequency of the fringes ($\approx$ 0.1 Hz) in this example is due mainly to the analytical frequency offset ε.

Thus, there are three primary observables to be obtained from the single-channel stopped fringes, fringe phase, maximum amplitude, and delay. The maximum amplitude (Eq. 14) leads to a determination of correlated flux or fringe visibility which can be used to investigate source structure. Single-channel fringe phase $\phi_f - \phi_m$ can only be determined to within an additive constant ($2n\pi$). For this reason, it only yields information concerning the time-varying components of the geometric delay, transmission media phase and instrumental phase. The third single-channel observable, the delay, is a sum of all group delay effects (geometric, transmission media, instrumental, clock synchronization). For sufficiently wide recorded bandwidths, the single-channel delay observable can yield useful information concerning all of these quantities.

[1] $\nu_g = \omega_a \dot{\tau}_g$

[2] Developed by D. S. Robertson and A. H. Legg of Weapons Research Establishment, Australia.

The techniques used to extract phase, amplitude, and delay will be discussed in the next three sections.

V. Fourier Analysis

After phase counter-rotation, the stopped fringes consist of sinusoidally varying curves of unknown frequency ($\approx \varepsilon$) and amplitude. Fourier analysis can be employed to extract these unknowns whenever the stopped fringes possess a sufficiently constant frequency and amplitude over the integration interval. The factors that cause the frequency and amplitude to vary will be discussed later in this section. Assume for the moment that the stopped fringes possess fairly constant amplitude and frequency so that Fourier analysis is useful.

Because of computation speed, the Fast Fourier Transform (FFT) is used for Fourier analysis. The FFT used in the present work can be expressed as the following discrete transform.

$$a_k = \frac{1}{2N}\sum_{t=0}^{N-1} g_t \exp\left(\frac{-i\pi \ell k}{N}\right) \qquad k = 0, 1 \cdots 2N-1$$

$$= \frac{1}{2N}\sum_{t=0}^{N-1} g_t \exp\left(-2\pi i f_k t_t\right) \tag{17}$$

where

$$t_t = \ell\, \Delta t_s$$

$$f_k = \frac{k}{2T}$$

$$T = N\Delta t_s$$

In these expressions, N is the number of fringe sample points in the integration interval T. The integration interval for the present 48-kbits/s recording system is usually the time span of one tape-pair (≈ 12 min). The input points g_t are given by the stopped fringe values computed in Eq. (12).

$$g_t = U_N(t_t, \tau_m) \qquad \ell = 0, 1 \cdots N-1 \tag{18}$$

where time (t_t) is measured relative to the beginning of the integration interval. Note that the frequency values (f_k) increment in steps of $1/(2T)$. (It should be noted that the normal FFT increments frequency in steps of $1/T$ which is sometimes inconveniently large. The normal FFT subroutines will perform the transform with twice the normal sample rate if the input array is doubled by filling the last N members with zeroes).

The single frequency response of the FFT can be determined by substituting a pure sinusoid with frequency f and phase β in Eq. (17).

$$g_t = A_T \cos\left(2\pi f \ell\, \Delta t_s + \beta\right) \qquad \ell = 0, 1, \cdots N-1 \tag{19}$$

The FFT modulus for this input function is given by

$$|a_k| \approx \frac{A_T}{4}\frac{\sin\left[\pi(k_f - k)/2\right]}{\pi(k_f - k)/2} \text{ for } |k_f - k| << 2N \tag{20}$$

where $k_f = 2fT$. Note that the frequencies k and k_f are in units of $1/(2T)$. As indicated by the $\sin(x)/x$ curve in Fig. 4, the FFT modulus $|a_k|$ peaks when k equals the input frequency. Note that the main lobe is four intervals wide. The first zeroes are separated from the principal maximum by $1/T$ in frequency. For a monochromatic input, the first side lobes should be attenuated by about $2/(3\pi)$ relative to the main lobe.

The data points in Fig. 4 are the FFT of the fringes in Fig. 3 for $\tau_V = 0$. The fact that the fringe FFT drops to zero within $1/T$ and also has side lobes of the correct size indicates that, at the spectral sensitivity of the transform ($\approx 200\ \mu$Hz), only one frequency is present.

After the FFT has been calculated for a given fringe curve, the FFT modulus is digitally searched for a maximum. After the main lobe is located, peak amplitude and center frequency are estimated by interpolation between the three main-lobe points or by a least-squares fit. In the least squares fit, the single-frequency response curve is typically fit to the points in the main lobe and two side lobes with the amplitude (A_T) and frequency (f) as solve-for parameters as indicated in Fig. 4.

Up to this point, we have assumed that the stopped fringes possess a constant amplitude and frequency over the integration period. In practice, both of these quantities change in time. The amplitude slowly changes because the radio source brightness transform and the system temperatures can sometimes change with time. Generally, these amplitude changes are negligible for integration times less than 10 min. The stopped fringe frequency, however, can change considerably in 10 min due to instrumental frequency instability, geometric delay model errors, and transmission media delays. If one of these factors causes frequency drifts across the integration interval (T) that are comparable to $1/T$, the FFT will spread out so that the FFT peak amplitude will underestimate the actual fringe amplitude. Expressed in terms

of phase, large phase deviations (~ 0.1 cycle) from linear behavior will cause loss of coherence in integration and therefore will diminish the peak response. If the frequency drifts are large compared to $1/T$, the FFT peak amplitude for weak sources can be so drastically reduced that the FFT signal is lost in the noise.

Rapid changes in frequency can sometimes be caused by rapidly changing troposphere delays at low elevation angles. This effect can generally be adequately removed by including an accurate troposphere correction in the model delay τ_m.

The magnitude of geometric frequency drifts can be bounded by means of the maximum values of the appropriate second partials, which for intercontinental observations at S-band are given by

$$\begin{aligned} \frac{\partial^2 \nu_g}{\partial x\, \partial t} &\lesssim \omega_e \left.\frac{\partial \nu_g}{\partial x}\right|_{\max} < 0.04\ \mu\text{Hz/m-sec} \\ \frac{\partial^2 \nu_g}{\partial \theta\, \partial t} &\lesssim \omega_e \left.\frac{\partial \nu_g}{\partial \theta}\right|_{\max} < 1.5\ \mu\text{Hz/(arc sec)-sec} \end{aligned} \tag{21}$$

where x, θ symbolize length and angle variables respectively and ω_e is Earth's rotation rate in radians/sec. For example, for a source error of 1 arc sec and an integration time of 100 sec, the geometric residual frequency would change by less than 0.15 mHz. Since the FFT single frequency response would be 10 mHz wide in this example, a frequency drift less than 0.15 mHz would only slightly decrease the FFT peak amplitude.

Instrumental instability can also cause frequency variations that reduce the FFT peak amplitude. Up to this point, we have only emphasized the largest component in the mixing signal, the linear term $\Delta\omega_a t$. In practice, actual mixing signals drift away from this ideal linear behavior by some amount, which has been collected in the phase term $I_a(t)$. These mixing signal drifts are usually due to frequency standard instabilities. One can easily estimate a typical phase (or frequency) drift for a given frequency standard if the stability specifications are available.

In summary, a Fourier transform of the stopped fringes serves two purposes in the present data reduction system. First, the FFT is used to detect the presence of fringes. The FFT reduces the detection problem to a simple search in the frequency domain. Secondly, once the FFT peak has been detected, the amplitude and frequency of the fringes can be estimated. These amplitude and frequency estimates are then used to initialize the phase tracking procedure, which will be described in the next section. The new estimates for amplitude and frequency produced by phase tracking are usually adopted as the final values. However, the FFT estimates for these quantities often serve as useful "quick-look" values.

VI. Phase Tracking

As indicated in the last section, FFT analysis can be used to determine the amplitude and frequency of the stopped fringes if they are "monochromatic" with constant amplitude over the integration interval. However, if nonlinear phase excursions are present, it is often desirable to extract the phase as a function of time. In addition, as we shall see, the two-channel approach to bandwidth synthesis requires phase extraction. Therefore, a technique called phase tracking was developed to extract the fringe phase. In this procedure, the time interval of interest (generally the FFT integration interval) is separated into subintervals with length Δt_ϕ (typically 1 to 100 sec). Each subinterval is fit successively by least squares with the sinusoid

$$f_s(t) = A_s \cos\left[2\pi\left(f_s t + \phi_s\right)\right] \tag{22}$$

where time t is zero at the beginning of each subinterval. With this definition, the phase ϕ_s denotes the phase at the beginning of the subinterval. In each subinterval, the amplitude (A_s), frequency (f_s), and phase (ϕ_s) are simultaneously varied in the least-squares fit. In the fit to each subinterval, the *a priori* amplitude and frequency are usually assigned the FFT values for the whole phase track period (≈ 10 min).

For the *first* interval, the *a priori* phase is determined by a least-squares search between 0–1 cycle with the amplitude and frequency fixed at the FFT values. After this initialization, a simultaneous least squares fit gives the amplitude, frequency, and phase (between 0–1 cycle) for the first interval.

For the *next and successive subintervals*, the *a priori* phase is found by adding the phase increment predicted by

$$\Delta\phi_s = f_{\text{FFT}}\, \Delta t_\phi \tag{23}$$

to the least-squares phase value for the preceding interval where f_{FFT} is the FFT frequency estimate. This projected phase estimate must be correct within about 0.2 cycle in order for the fit to succeed. (When frequency changes across the FFT integration interval are large, the frequency and phase of a given subinterval should be initialized with the least-squares frequency of the pre-

ceding subinterval provided the SNR is adequate.) After the simultaneous three-parameter fit for each subinterval, the parameter covariance errors are calculated on the basis of the actual RMS fringe residuals. Thus, the phase track output consists of the amplitude, frequency, phase, covariance errors, and RMS fringe residual for each subinterval.

The length of the subintervals should be made sufficiently small to reveal nonlinear trends in the phase. When nonlinear phase trends are present, the maximum subinterval length is defined by

$$\Delta t_\phi < \frac{\sigma_\phi}{\Delta f_s} \tag{24}$$

where σ_ϕ is the phase covariance error due to system noise, and Δf_s is the frequency change over the subinterval. That is, the phase effects of frequency drifts across a subinterval should be small compared to phase measurement precision. The minimum subinterval length is approximately equal to the time required for 0.5 cycle of fringe phase or by SNR limitations.

After the phase for each subinterval has been extracted, the phase values for the phase track period are given the proper sign by appropriately removing the analytical offset εt (see Eq. 8). The expected behavior of these corrected phase values, called residual phase $\Delta\phi_a$, is given by the expression

$$\Delta\phi_a = \Delta\omega_a t + \omega_a \Delta\tau_r' + I_a + R_a + C_a \tag{25}$$

If the delay model is sufficiently accurate and the frequency system is sufficiently stable, the residual phase will, to good approximation, vary linearly in time over the phase track interval (≈ 10 min). For this reason the residual phase values are fit by least squares with a straight line over the interval. In some cases, the fit slope, which is the "average" residual fringe frequency for the fit interval, is used as the "phase observable" for that interval. However, when large nonlinear phase excursions are present over a fit interval, the residual phase should be analyzed, since a single frequency clearly cannot describe nonlinear phase changes.

In some applications, when one source is observed more or less continuously for hours, the phase can be connected between phase track periods (in analogy with the phase projection described above) so that one obtains the connected phase over a long time interval (1 to 8 hours). When phase can be connected over hours, low magnitude (≈ 0.1 cycle) short term (≈ 10 min) phase excursions are less damaging. For example, local derivatives of the indicated excursions produce frequency noise of the order of 0.1 mHz which corresponds to 20 cm in equivalent baseline error for S-band observations. On the other hand, a grand fit to hours of connected phase data in this example will experience only 0.1 cycle (1 cm at S-band) of phase noise.

An example of a least-squares fit of a phase-track sinusoid is shown in Fig. 3 for several delay offsets. Only a fraction of the first subinterval (30 out of 50 sec) is displayed in the figure. Figure 5 shows the residual phase values obtained by phase-tracking the $\tau_V = 0$ fringes in Fig. 3 over 600 sec. Note that the 0.1-Hz analytical offset has been removed. The residual fringe frequency $\Delta\dot{\phi}_a$ is a consequence of all of the terms listed in Eq. (25). As one would require, there is excellent agreement between the fringe frequency values obtained by phase-tracking in Fig. 5 and by Fourier transform in Fig. 4 (after the FFT result has been corrected for the 100-mHz analytical offset). The amplitude values obtained by phase-tracking the fringes in Fig. 3 are shown in Fig. 6. The amplitude value for each delay offset τ_V is an average of the twelve amplitudes obtained from the twelve phase-track subintervals. Note the excellent agreement between the amplitudes obtained by phase-tracking ($\tau_V = 0$ case in Fig. 6) and by Fourier analysis in Fig. 4. As indicated in Fig. 6, the amplitude variation versus time offset has been fit with the $\sin(x)/x$ curve that would be generated by an ideal rectangular bandpass that is 24 kHz wide. The deviation of data points from the $\sin(x)/x$ curve is primarily due to the nonideal response of the actual system bandpass. In the least-squares fit, the center and amplitude of the $\sin(x)/x$ curve are used as solve-for parameters. The least-squares values for amplitude and center delay are a measure of the maximum amplitude and single-channel delay for the phase-track interval. (The delay and amplitude errors quoted for the example in Fig. 6 include the modeling error associated with the inadequate $\sin(x)/x$ curve. It should be noted that a more accurate delay curve model based on system bandpass measurements would improve the delay and amplitude precision considerably. For the example in Fig. 6, the delay uncertainty due to system noise alone would be about 150 nsec).

After a given time interval has been phase-tracked, the most important output quantities are the amplitude and phase for each subinterval. For the present 48 kbits/s system, only the phase values that are generated by the "peaked" fringes [i.e., $2W_B \Delta\tau_r < 1$] are retained for subsequent data analysis. (The slight statistical advantage gained by processing more delay offsets is greatly out-

weighed by the increased computation costs for this system). The fringe phase is an important observable containing valuable information concerning geometric quantities as well as transmission media and instrumental effects. As indicated in the next section, phase values measured for two separate channels can be combined by a procedure known as bandwidth synthesis to extract the delay. The amplitude values produced by the peaked fringes are retained for use in source structure calculations. If the fringes are phase-tracked or Fourier-analyzed for a range of delay offsets (τ_V), the amplitude variation as a function of delay can be analyzed to extract the single-channel delay.

VII. Bandwidth Synthesis

This section is devoted to a discussion of time delay measurements with emphasis on two-channel bandwidth synthesis.

As indicated in Section VI for a single band-limited channel, fringe phase can be determined over the phase-track interval except for an overall $2n\pi$ ambiguity. Therefore, with regard to single-channel phase, only the time-varying components carry information that may be readily analyzed. Since the z-component of the baseline (component along Earth's spin axis) enters the phase as a constant effect for a given source (Ref. 4), this $2n\pi$ phase uncertainty increases the difficulty of determining the z-component from single-channel phase. For this reason, delay measurements are desirable for three-dimensional baseline determination. Furthermore, the extra information carried by the delay observable strengthens the solution of the general multiparameter fitting procedure involving sources, baselines, and Earth orientation factors. For example, the delay observable removes the well-known singularity problem (unknowns > independent equations) and the zero-declination weakness associated with fits to fringe phase (or fringe frequency). For these reasons, a capability for precisely measuring delay becomes very desirable.

In general, the precision of delay measurements improves as the range of the observed frequencies increases (see Ref. 1 and Eq. 27). One way to increase the frequency range is to increase the recorded bandwidth. However, practical considerations regarding the size of the instantaneous record rate (cross-correlation cost and complexity, recorder availability) place the present system bandwidths at 2 MHz or less. Delay measurements with high precision (≈ 60 psec $\simeq 2$ cm) require much larger bandwidths than 2 MHz (Ref. 1). Therefore, in order to increase the frequency range further, a technique known as bandwidth synthesis has been employed. In this technique, one combines, either directly or indirectly, the phase information provided by a few band-limited channels whose separation in frequency is large compared to the single-channel bandwidth. In the original application of this technique (Ref. 5) six channels of radio noise were recorded in a time-shared mode. In that system the six channels equally share the total statistics allowed by the instantaneous record rate. However, the statistics associated with the two outer channels, separated by the greatest frequency interval, primarily determine the final precision of the delay observable. The inner channels serve mainly to resolve ambiguities in the delay determination. That is, with a six-channel experiment, the *a priori* delay can be much more uncertain than the *a priori* delay in a two-channel experiment with the same total frequency spread. However, in measurements that involve sufficiently precise *a priori* delay information, inner channels serve no function and are a waste of statistics.[3] In those cases, only the two outer channels should be measured, so all of the statistical strength of the measurement contributes to the final delay precision. An example of such a measurement situation would be a set of short baseline (< 200 km) experiments designed to frequently monitor small baseline changes due to tectonic motion. The delay observable is not greatly corrupted by transmission media because of differential cancellation over short baselines. Furthermore, delays for short baselines are less sensitive to angular errors in Earth orientation and source locations. Therefore, if sufficiently precise values for source locations and Earth orientation are gathered from other work, the *a priori* delay can be calculated with sufficient accuracy to allow two-channel ambiguity resolution. (If the baseline is fairly uncertain initially, one can make one or two preliminary measurements with closely spaced channels to lower the baseline uncertainty.) See Ref. 6 for a feasibility demonstration experiment for such a system. In some radio interferometry applications the two-channel approach is not adequate. An example would be a set of experiments that are corrupted by uncalibrated ionosphere delays that are large compared to the ambiguity level associated with the outer-channel separation.

In the remainder of this section, two-channel bandwidth synthesis will be analyzed. In principle, the multichannel system is also treated since the two-channel approach can be applied successively to channel pairs beginning with the two most closely spaced channels. That is, one can refine the *a priori* delay on the basis of the first two channels and proceed to the next larger sepa-

[3]This point was originally suggested by P. F. MacDoran.

ration and so forth. However, in the original application (Ref. 5) of the multichannel approach, the delay was obtained by summing the fringes of the various channels to obtain a delay response curve. This approach requires calibration of the relative phase of the various channels. As we shall see, the two-channel approach treats the instrumental phase as a solve-for parameter and thereby eliminates the need for relative phase calibration. That is, the only requirement placed on the instrumental phase by the two-channel technique is that the instrumental phase should exhibit stability with respect to some simple functional form—a constant, linear drift, etc.

An example of an instrumental configuration designed[4] for optimum phase stability in two-channel observations is shown in Fig. 7. In this system, a 10-MHz signal from the H-maser is converted to a 2240-MHz first local oscillator (LO) signal by using only multipliers: the standard $\times 4$ $\times 8$ multipliers and a new $\times 7$ multiplier. The $\times 7$ multiplier was designed and constructed[5] in order to avoid the use of a synthesizer. The $\times 7$ multiplier converts the input sinusoid to a square wave and then filters and amplifies the seventh harmonic.

In order to achieve maximum channel separation and better delay precision, the traveling wave maser (TWM) receiver bandpass was broadened by retuning the trim coil currents. In the retuned state, the receiver exhibited ample amplification over a 40-MHz interval (2270 to 2310 MHz) while maintaining an operating system noise temperature less than 30 K. Therefore, after mixing with the first LO signal at 2240 MHz, the edges of the receiver passband were placed at 30 and 70 MHz. However, this frequency spread exceeded the bandpass of the standard first mixer/preamp which possesses adequate gain only over 45 to 55 MHz. Consequently, the standard mixer/preamp was replaced with a similar module with a bandpass between 10 and 160 MHz, thereby making the system bandpass TWM-limited. The IF passband is then filtered into two channels—one centered at 30 MHz and the other at 70 MHz. Each channel is mixed with a 20-MHz signal derived from the hydrogen maser and each mixer response is appropriately filtered to place both channels at 50 MHz. At this point, each channel is transferred on alternate seconds to the video converter. The video converter mixes the input IF signal to baseband with a 50-MHz signal derived from the hydrogen maser. This time-shared baseband signal is passed through a 24-kHz bandpass for digital sampling and recording at a 48-kbit/sec rate. Note that the instrumental phase of this system relies exclusively on multipliers and H-maser frequency standards. [With this configuration, the differential phase noise was *less than* 0.008 cycles between the two channels for 700 second integration times (Ref. 6). Phase noise at the 0.008 cycle level corresponds to 200 psec (6 cm) of delay noise for a 40-MHz synthesized bandwidth.]

An example of stopped fringes generated by the above configuration is shown in Fig. 8. Note that alternate seconds clearly contain distinct fringes. The phase tracking technique outlined earlier can easily be modified to independently extract the phase of each fringe curve. Phase values obtained from the example fringes in Fig. 8 are shown in Fig. 9. The analytical offset ε has been removed after assigning the phase the proper sign. The small nonlinear phase excursions (≈ 0.03 cycle) could possibly be due to ionosphere effects. Note that the excursions are nearly identical in the two channels so that they nearly cancel in the delay calculation that follows. As indicated by Eq. (25), these phase values are theoretically represented by the expressions

$$\Delta\phi_a = \omega_a \Delta\tau_r' + R_a + \Psi_a + C_a \tag{26}$$

$$\Delta\phi_b = \omega_b \Delta\tau_r' + R_b + \Psi_b + C_b$$

where the subscript $a\,(b)$ denotes channel $a\,(b)$. In this expression, all instrumental phase effects have been included in Ψ_a and Ψ_b. The measured delay ($\Delta\tau$) may be extracted by combining the phase values as follows:

$$\Delta\tau \equiv \frac{\Delta\phi_a - \Delta\phi_b}{\omega_a - \omega_b} \tag{27}$$

In calculating $\Delta\tau$, one can assume that the frequency separation $\omega_a - \omega_b$ is essentially perfectly known ($\Delta f/f \approx 10^{-12}$). As described below, care must be taken to assign the correct value of $2n\pi$ to $\Delta\phi_a - \Delta\phi_b$. The expected behavior of $\Delta\tau$ is given by the expression

$$\Delta\tau = \Delta\tau_r' + \frac{\Psi_a - \Psi_b + C_a - C_b}{\omega_a - \omega_b} \tag{28}$$

We have assumed that the brightness transform phase R_a changes a negligible amount between channels.

The charged particle phase difference $C_a - C_b$ can be reduced to delay τ_c as follows. It can be readily shown that the charged-particle phase shift for channel x is given by expression (Ref. 7):

$$C_x = \frac{P_T}{\omega_x} \tag{29}$$

[4]This configuration was designed by D. J. Spitzmesser.

[5]Designed and constructed by R. L. Sydnor.

where

$$P_T = \frac{e^2}{2\pi m_e c}(N_1 - N_2)$$

In this expression, c is the speed of light and e and m_e are the charge and mass of the electron in mks units. Furthermore, $N_1 - N_2$ is the difference of the electron columnar content (number/area) along the two ray paths. The phase shift C_x is in cycles, and the frequency ω_x is in Hz. Based on Eq. (29), the charged-particle phase difference becomes

$$\begin{aligned} C_a - C_b &= \frac{P_T}{\omega_a} - \frac{P_T}{\omega_b} \\ &= -\frac{P_T}{\omega_a^2}(\omega_a - \omega_b) \text{ for } |\omega_a - \omega_b| << \omega_a \\ &= \tau_c(\omega_a - \omega_b) \end{aligned} \tag{30}$$

where $\tau_c = -P_T/\omega_a^2$ is the total delay due to charged particles. The expected behavior of the measured delay is then given by

$$\Delta\tau = \Delta\tau_r + \frac{\Psi_a - \Psi_b}{\omega_a - \omega_b} \tag{31}$$

where

$$\begin{aligned} \Delta\tau_r &= \Delta\tau_r' + \tau_c \\ &= \tau_g + \tau_I + \tau_c + \tau_t - \tau_m \end{aligned}$$

If the model delay is sufficiently accurate, and if the frequency systems are well calibrated, the measured delay $\Delta\tau$ will be constant (within the delay noise) over considerable time intervals (≈ 10 min). In this case, the delay values can be averaged over the interval. The delay values obtained from the phase plots in Fig. 9 are shown in Fig. 10 along with the average delay $\overline{\Delta\tau}$ for the whole 10-min interval. The delay error estimate in Fig. 10 is the uncertainty due to system noise.

When the phase values from the two channels are combined in Eq. (27), care must be taken to avoid $2n\pi$ ambiguities. That is, the difference $\Delta\phi_a - \Delta\phi_b$ must be assigned the proper number of integer cycles. A procedure with which $2n\pi$ ambiguities can be resolved will be discussed in the next four paragraphs.

Note that the phase difference is theoretically a sum of two terms.

$$\Delta\phi_a - \Delta\phi_b = (\omega_a - \omega_b)\Delta\tau_r + \Psi_a - \Psi_b \tag{32}$$

The instrumental phase term $\Psi_a - \Psi_b$ usually is not constant due to differences in the frequency systems at the two stations. If the frequency systems are very stable ($\Delta f/f \approx 10^{-14}$ for the better H-maser standards), this instrumental phase difference can be treated as a constant plus a linear drift in time. The linear drift is due primarily to the rate difference of the frequency standards. For good frequency standard calibration accuracies ($\Delta f/f \approx 10^{-12}$), the rate, $\dot{\Psi}_a - \dot{\Psi}_b$, will be about 40 μHz for a 40 MHz channel separation. At this rate, the instrumental phase difference will change only one cycle in 8 hours.

The maximum magnitude of the first term $(\omega_a - \omega_b)\Delta\tau_r$ is determined by the residual delay $\Delta\tau_r$, which may be estimated as follows. The maximum geometric delay errors are readily calculated using the maximum partial magnitudes and the *a priori* uncertainties in the geometric delay parameters (baseline, source location, UT1 etc.). The maximum values of the sensitivity partials (Ref. 4) for the geometric delay over an intercontinental baseline ($\approx 10{,}000$ km) are given by

$$\frac{\partial\tau_g}{\partial x} \sim 3 \text{ nsec/m} \qquad \frac{\partial\tau_g}{\partial\theta} \sim 150 \text{ nsec/arc sec} \tag{33}$$

where x and θ symbolize length and angle parameters respectively. For example, if the *a priori* source position is uncertain at the 2 arc sec level, this uncertainty will contribute less than 300 nsec to $\Delta\tau_r$. The magnitudes of transmission media calibration errors can usually be estimated once the calibration technique is selected. The terms in the delay that are constant at the level required for ambiguity resolution can be neglected at this stage. We will assume cable delays, bandpass group delays, etc., are constant at this level. These constant terms, as we shall see, are truncated or absorbed in the constant offset. After one has determined the maximum value of $\Delta\tau_r$ due to uncertainties in the variable components, the channel separation $\omega_a - \omega_b$, is selected so that, in the worst case, the term $(\omega_a - \omega_b)\Delta\tau_r$ is less than 0.2 cycle in magnitude. With this design, this first term will scatter more or less randomly between ± 0.2 cycle as one measures the delay for various sources in various directions.

Therefore, the phase difference $\Delta\phi_a - \Delta\phi_b$ consists of two terms—a slowly changing but continuous instrumental phase term plus a delay term that varies more or less randomly between ± 0.2 cycle when changing from source to source. Since the rate of the instrumental term is usually not exactly known, it may be treated as follows. We will assume for the moment that the rate is small (~ 40 μHz). The average phase difference $\Delta\phi_a - \Delta\phi_b$ for the *first* radio source (1 to 10 minutes duration) is assigned the particular value of $2n\pi$ required to place $\Delta\phi_a - \Delta\phi_b$ between 0 to 1 cycle. This initialization procedure is justi-

fied by the fact that delay will always possess an unknown additive constant that will be a solve-for parameter. By this initialization, the level of the constant has been chosen to place the *first* delay value in a specified range. This delay truncation means that clock synchronization and constant instrumental delays cannot be determined by two-channel bandwidth synthesis unless elaborate instrumental phase and delay calibrations are performed to initialize the instrumental constant to within $2n\pi$. Once the first delay has been defined, care must be taken to assign the correct value of $2n\pi$ to subsequent delay values. If the instrumental phase, $\Psi_a - \Psi_b$, is slowly varying ($\sim 40\ \mu$Hz) then it will change by a fraction (~ 0.03) of a cycle before the next delay value is obtained a short time (≈ 10 min) later. If this is the case, the next phase difference must be within ± 0.2 cycle of the first difference provided the residual delay $\Delta\tau_r$ falls in the expected range. In this manner, the $2n\pi$ factor for each delay can be determined by comparison with the preceding phase difference.

Up to this point, we have assumed the instrumental rate $\dot{\Psi}_a - \dot{\Psi}_b$ is small ($\sim 40\ \mu$Hz). When this assumption is not satisfied, several courses of action are available. The most reliable but time-consuming frequency calibration involves an independent multiparameter fit to the single-channel phase (fringe frequency) observables to obtain the frequency offset at RF. The resulting offset can be easily scaled from RF to the synthesized bandwidth. No time is wasted by this procedure, since an independent fringe frequency solution should normally be performed as a check on the delay solutions. Another easier frequency calibration technique is to use a well-known source as a calibrator provided other geometric fringe frequency uncertainties are sufficiently small. The frequency standard rate difference has to be determined to within only about 2 MHz at S-band to allow the ambiguity resolution steps to proceed for a 40-MHz synthesized bandwidth. Once the oscillator offset is approximately known, the phase differences, $\Delta\phi_a - \Delta\phi_b$, can be corrected to remove the rapid linear drift. The ambiguity resolution process can then be applied, as outlined above, to these more slowly varying corrected phase differences.

Once the single-channel phase values and delay values have been determined for all observations, these observables can be fit simultaneously by a weighted least-squares technique to determine the source locations, baseline and Earth orientation factors. If the delay model τ_m used in data reduction is considered inappropriate for the least-squares fit, then one can add τ_m to the measured delay $\Delta\tau$ to obtain the total measured delay free of theoretical models.

VIII. Summary

In this report, the practical aspects of the JPL long baseline interferometry data reduction procedure have been described. The steps include bit stream manipulations, fringe stopping, Fourier analysis and phase-tracking. The most important output of these steps is fringe amplitude and fringe phase. Fringe phase values measured for two separate channels are combined by a procedure known as bandwidth synthesis to precisely extract delay. For less precise delay measurements, fringe amplitude variation versus model delay can be used to extract single-channel delay. Peak fringe amplitude can yield valuable information concerning source structure.

References

1. Thomas, J. B., "An Analysis of Long Baseline Radio Interferometry," in *The Deep Space Network Progress Report*, Technical Report 32-1526, Vol. VII, p. 37. Jet Propulsion Laboratory, Pasadena, Calif., Feb. 15, 1972.

2. Thomas, J. B., "An Analysis of Long Baseline Radio Interferometry, Part II," in *The Deep Space Network Progress Report*, Technical Report 32-1526, Vol. VIII, Jet Propulsion Laboratory, Pasadena, Calif., April 15, 1972.

3. Van Vleck, J. H., and Middleton, D., "The Spectrum of Clipped Noise," *Proc. IEEE*, Vol. 54, No. 1, p. 2, January 1966.

4. Williams, J. G., "Very Long Baseline Radio Interferometry and Its Sensitivity to Geophysical and Astronomical Effects," in *The Deep Space Network*, Space Programs Summary 37-62, Vol. II, p. 49. Jet Propulsion Laboratory, Pasadena, Calif., March 31, 1970.

5. Rogers, A. E. E., "Very Long Baseline Interferometry With Large Effective Bandwidth for Phase-Delay Measurements," *Radio Sci.*, Vol. 5, No. 10, p. 1239, October 1970.

6. Thomas, J. B., et al., "Radio Interferometry Measurements of a 16-Kilometer Baseline with 4 Centimeter Precision" (to be published).

7. MacDoran, P. F., "A First Principles Derivation of the DRVID Charged Particle Calibration Method," in *The Deep Space Network*, Space Programs Summary 37-62, Vol. II, p. 28. Jet Propulsion Laboratory, March 21, 1970.

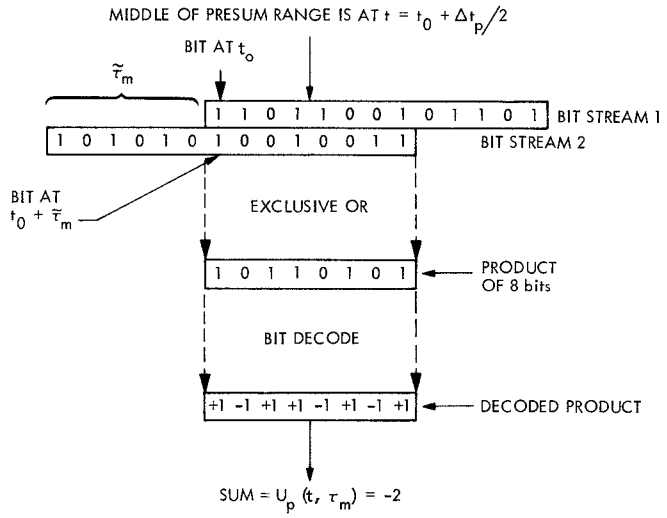

Fig. 1. Example of bit multiplication and presum

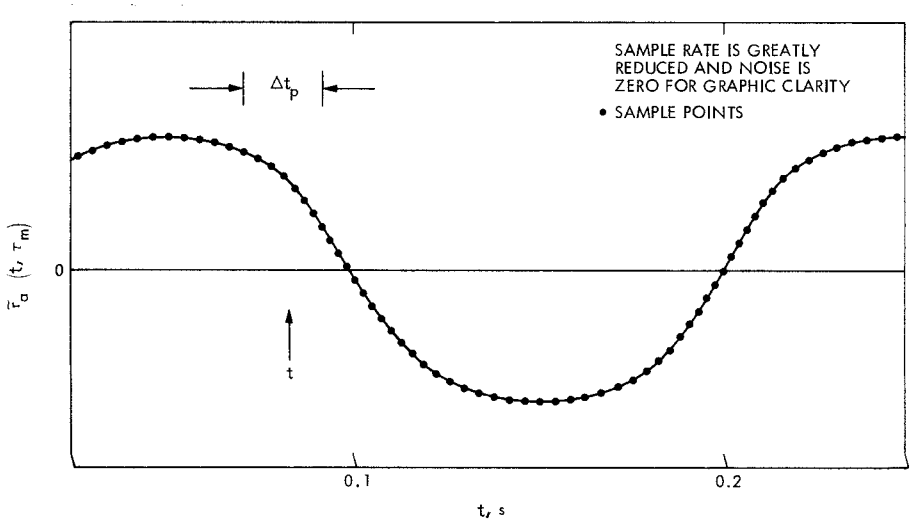

Fig. 2. Schematic example of presum time interval

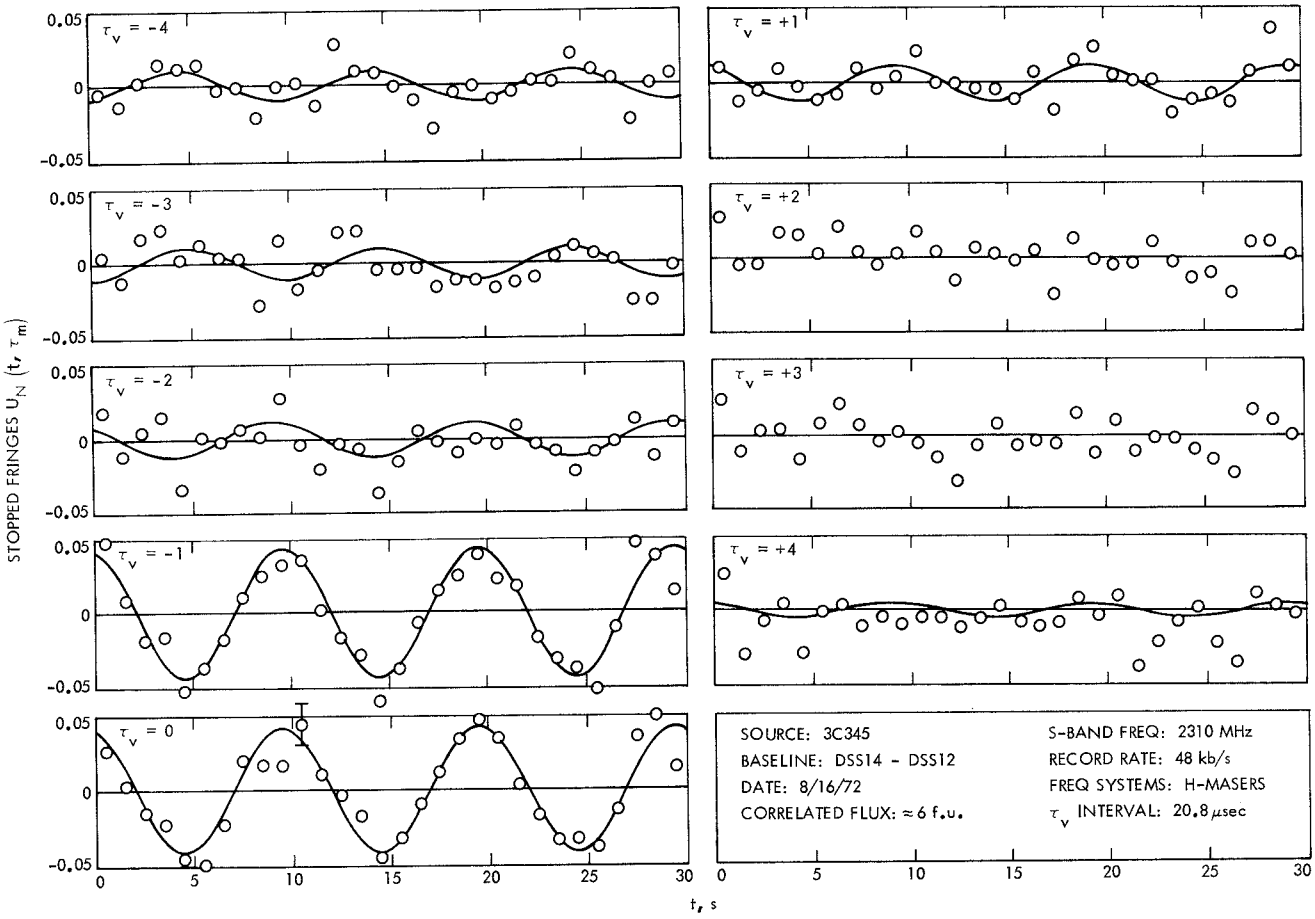

Fig. 3. Example of stopped fringes

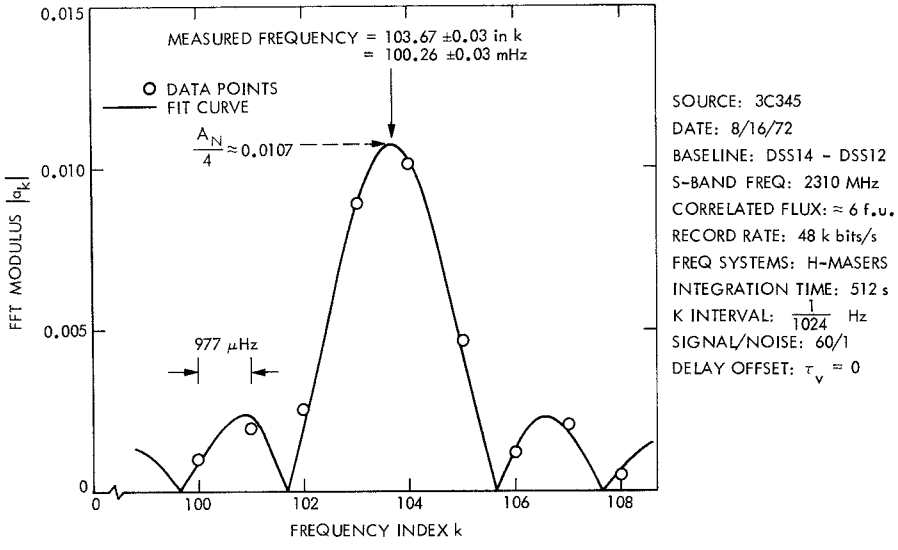

Fig. 4. Fourier transform of stopped fringes

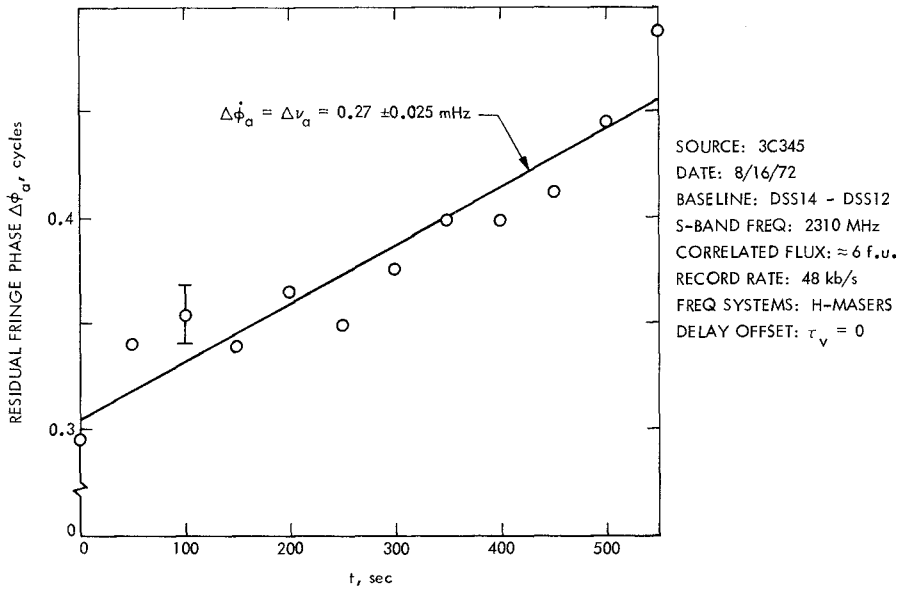

Fig. 5. Residual fringe phase plot

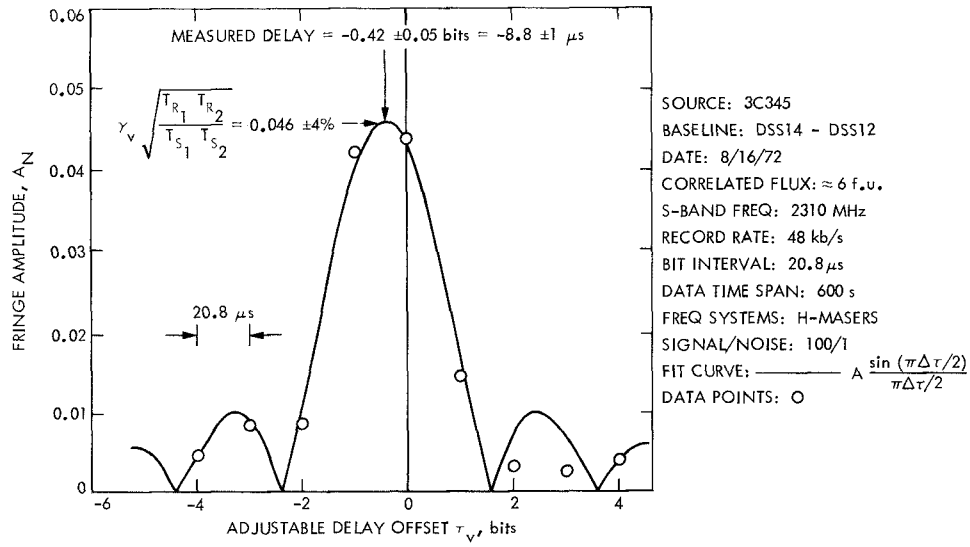

Fig. 6. Example of a delay curve

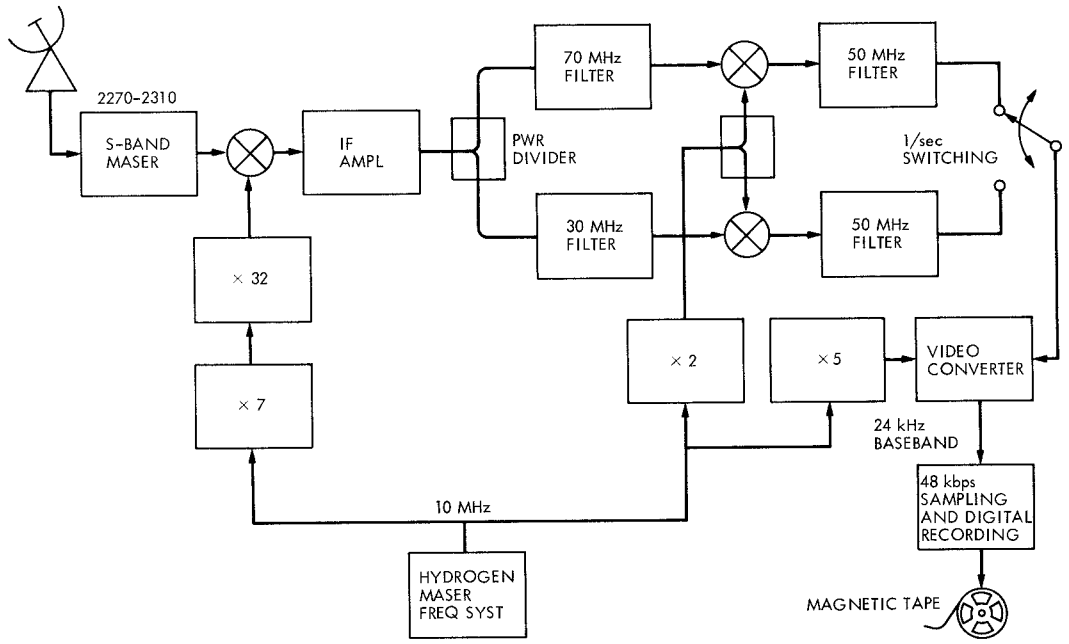

Fig. 7. Deep space station configuration for 40-MHz bandwidth synthesis

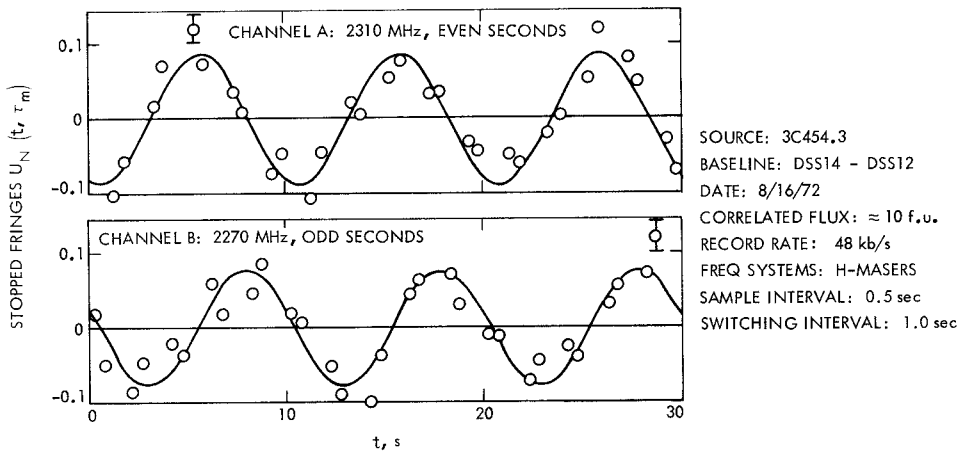

Fig. 8. Stopped fringes for two-channel bandwidth synthesis

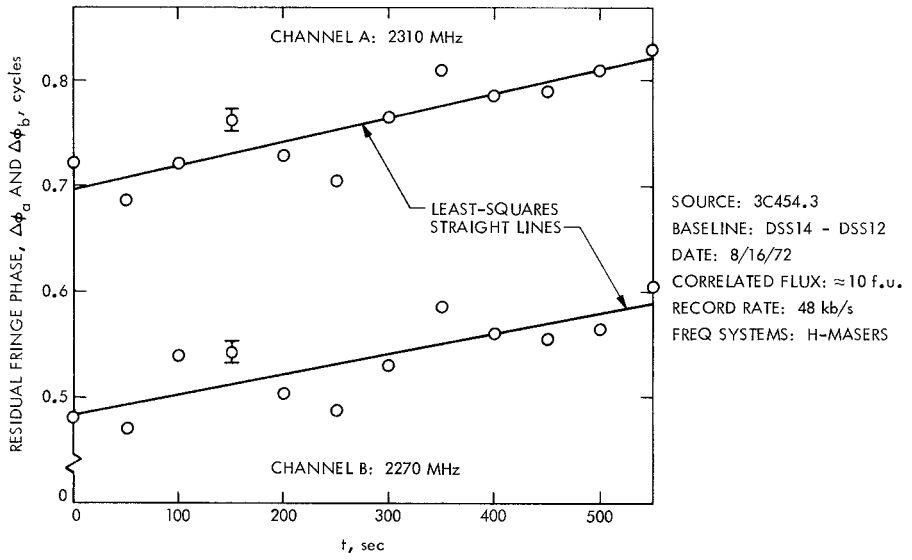

Fig. 9. Fringe phase values for two-channel bandwidth synthesis

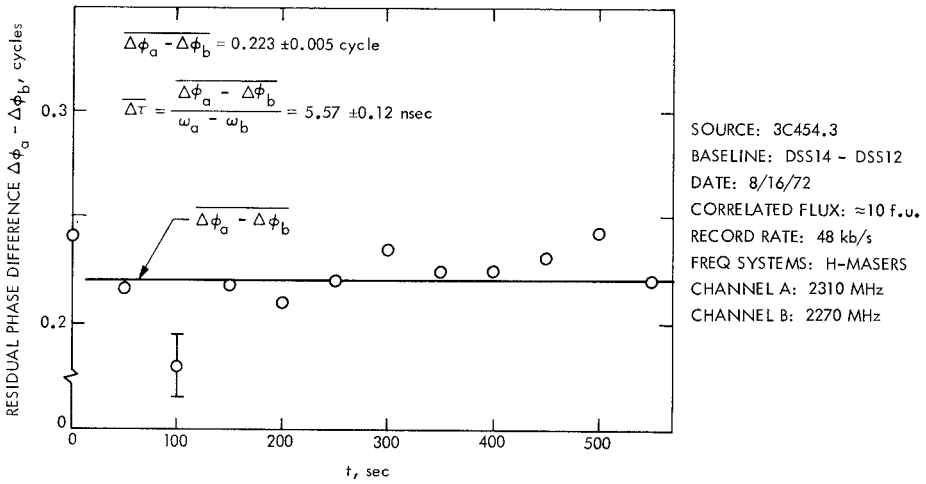

Fig. 10. Example of a delay calculation with two-channel bandwidth synthesis